PHILOSOPHICAL MAGAZINE A, 1997, VOL. 75, NO. 2, 443–459

Mechanism of intense shear failure in Ni_3Al single crystals

By MING DAO, BIMAL K. KAD and ROBERT J. ASARO

Department of Applied Mechanics and Engineering Sciences, 0411
University of California, San Diego, La Jolla, California 92093, USA

[*Received 5 May 1996 and accepted in revised form 24 June 1996*]

ABSTRACT

Localized shear bands, with minute misorientations off the slip plane, cause sharp failures in Ni_3Al single crystals that fail after elongation exceeding 70–80% in room-temperature tensile tests. An explanation for intense slip plane shear failure, consistent with prior experimental observations, is proposed. Prior electron microscopy evidence obtained by Horton, Baker and Yoo of decreasing antiphase-boundary energy in highly deformed slip bands is employed to suggest a highly localized order–disorder transition. This shear-strain-induced slip-plane disordering provides the essential mechanism to lower the work-hardening rate to zero or negative values. A decreasing work-hardening rate sustains persistent shear localization, ultimately leading to failure. This mechanism is suggested to be applicable to other ordered crystals.

§ 1. INTRODUCTION

1.1. *Background*

Fcc-based ordered $L1_2$ Ni_3Al alloys are extremely ductile in the single-crystal form, exhibiting room-temperature tensile strains of 70–80% prior to failure. Despite this high tensile ductility of Ni_3Al single crystals, the failure surfaces exhibit neither void coalescence nor typical cup-cone fractures of fcc alloys of aluminium, nickel, etc. Instead, the ambient temperature failures are highly localized events, often knife edge sharp (fig. 1) and nearly parallel to the primary slip plane.

Localized deformation events such as necking and shear banding are entirely natural inevitable outcomes of finite deformation of ductile crystalline materials. Shear bands, for example, can form within defect-free single crystals that display positive hardening in both single-slip and multiple-slip modes (Asaro and Rice 1977, Asaro 1979, Peirce, Asaro and Needleman 1983, Dao and Asaro 1993). Carefully designed experiments have repeatedly shown that shear bands form in many crystalline solids, with the material inside the bands undergoing positive strain hardening, at least at the initiation stage (Elam 1925, Beevers and Honeycombe 1962, Price and Kelly 1964, Chang and Asaro 1981, Harren, Dève and Asaro 1988). The attainment of the localized deformation mode, in this case, is often caused by the decreasing (positive) strain-hardening rate with strain accumulation (Asaro and Rice 1977, Asaro 1979, Peirce *et al.* 1983, Dao and Asaro 1993) (fig. 2(*a*)).

Localization may also be associated with material changes or imperfections which lower the strength level or work-hardening capacity. For example, adiabatic heating effects at high strain rates are known to cause shear bands (Duffy 1991, Gilman 1994). Radiation-damaged materials are observed to develop soft

Fig. 1

(*a*)

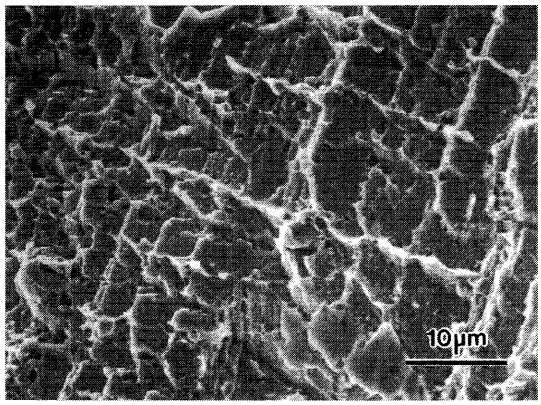

(*b*)

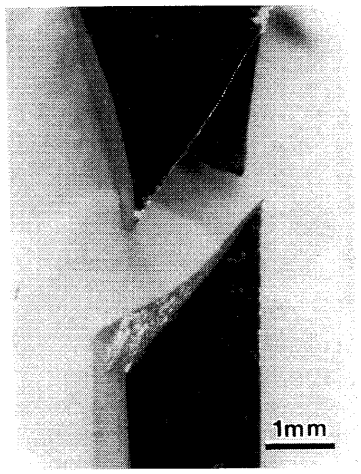

A ductile failure by intense shear localization in a single crystal of Ni_3Al deformed in tension at room temperature: (*a*) the fracture surface under scanning electron microscopy; (*b*) the failed tensile specimen. The tensile axis is [321].

Fig. 2

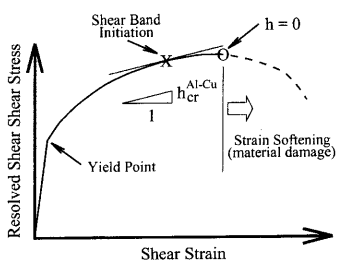

(a) Al-Cu Single Crystal

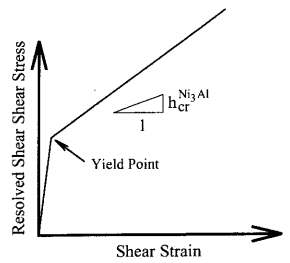

(b) Ni_3Al Single Crystal

Schematic drawings of the critical hardening h_{cr} against shear stress–shear strain curve for (*a*) Al–Cu and (*b*) Ni_3Al single crystals.

'channels' with easy slip caused by the sweeping up of point-defect debris by moving dislocations (Wechsler 1973).

The relation between deviations from the Schmid rule of a critical resolved shear stress and localization of plastic deformation in ductile single crystals was first studied by Asaro and Rice (1977). In this they recognized that, whereas the Schmid rule, which states that yielding occurs on a slip system when the resolved shear stress *alone* on that system reaches a critical value, is often a good approximation for simple crystals, deviations from it are inevitable. For example, ordered Ni_3Al (Paidar, Pope and Vitek, 1984) and ordered Ni_3Ga (Takeuchi and Kuramoto, 1973) are known for their *deviations from Schmid's rule* or *non-Schmid effects*, where stress components other than the resolved shear stress also contribute to the plastic shear deformation. Cross-slip is one of the most important micromechanical precesses that can result in significant non-Schmid effects, at least for ordered Ni_3Al and Ni_3Ga single crystals (Paidar *et al.* 1984).

1.2. *Statement of the problem*

Strain localizations are a natural consequence of deformation, particularly in alloys with a saturation work-hardening curve, deformed to large strains. However, it is not immediately obvious why such localizations persist in ordered Ni_3Al at room temperature, particularly their alignment with the primary slip plane, when it exhibits large positive, nearly linear work-hardening characteristics (Aoki and Izumi 1978a, b).

Furthermore, the incidence of large plastic strain prior to failure, ensures that large lattice rotations must occur to activate conjugate slip, irrespective of the initial $\langle 321 \rangle$ tensile axis, designed to promote single slip. However, Aoki and Izumi (1978 b) report significant tensile axis overshoots across the [001]–[111] symmetry line and the primary slip system continues to operate until $\tau^{(c)}/\tau^{(p)} \approx 1{\cdot}44$, where $\tau^{(c)}$ and $\tau^{(p)}$ are the resolved shear stresses on the conjugate and primary slip systems respectively. The specific mechanisms responsible for the relative softer response of the primary (or the relative harder response of the conjugate) slip system are currently unknown. While nominal overshoots (2–4°) in disordered crystals are attributed to a higher latent hardening on conjugate slip systems, the large overshoots observed in Ni_3Al remain a mystery.

A persistent shear band can only appear when hardening rate h is relatively low, that is approaching zero (Dao and Asaro 1996a, b). For single crystals undergoing single slip, Asaro and Rice (1977) prescribed a critical hardening rate criteria (i.e. $h \leqslant h_{cr} \rightarrow$ shear band) for shear localization nearly parallel to the slip plane. Asaro (1979), and later Dao and Asaro (1993), expanded this original effort to similarly prescribe the h_{cr} criteria for multiple slip. In the latter work, h_{cr} criteria includes positive temperature-dependent terms and is derived from non-Schmid considerations of conjugate and cube slip, in the specific case of Ni_3Al. Localizations are exacerbated when the actual work-hardening rate $h < h_{cr}$, where both h and h_{cr} are temperature dependent. In crystals with $\langle 321 \rangle$ tensile axis oriented for single slip, the absence of non-Schmid effects precludes all localization unless $h \leqslant 0$, a condition clearly not met in ambient-temperature single-crystal tests. Looking ahead to table 2 and §3.1, we note that, in fact, h_{cr} is very low while h is close to peak values at ambient temperatures in Ni_3Al, such that non-Schmid effects *alone* cannot explain intense shear failures. The specific problem therefore, as schematically shown in fig. 2(*b*), is to explore possible mechanisms to explain experimental

observation of persistent localizations, and subsequent knife edge failures, where the apparent hardening rate $h \gg h_{cr}$ before the sudden load drop (i.e. failure).

1.3. *Solution objectives and concepts*

In the current context of ordered intermetallics, we explore the notion that the incidence of macroscopic or localized order → disorder transition may provide plausible means for the loss in the material's work-hardening capacity. This order–disorder state in Cu_3Au, isostructural with Ni_3Al, has been previously employed to explore specific mechanical (flow stress and work hardening) as well as thermophysical (diffusion and resistivity) responses, and has advanced our basic understanding of intermetallic alloys and properties. For example, Sachs and Weerts (1931) demonstrated nearly 65 years ago, followed by Vidoz, Lazarevic and Cahn (1963), Davies and Stoloff (1963, 1964), and M. J. Marcinkowski and H. Chessin (1963, unpublished work) that fully ordered Cu_3Au exhibits a lower initial flow stress, and strain hardens more rapidly than the same alloy in the macroscopically disordered state (fig. 3). Unfortunately, bulk Ni_3Al is not known to exist in the disordered state, and thus any direct comparison between the work-hardening behaviours of the ordered and disordered states is not feasible.

However, looking ahead to fig. 7, Horton, Baker and Yoo (1991) report microscopy evidence for 'localized' slip plane disordering in stoichiometric Ni_3Al where, in the extensively deformed slip bands, the separations between superpartials become progressively larger until uncoupling occurs. In an earlier study, Baker, Horton and Schulson (1987) also observed widely separated (50 nm) and bowed (scalloped) superdislocation partials in the slip bands. Analogous to the case of Cu_3Au (Audero, Victoria and Vidoz, 1969), the uncoupling of superpartials is construed as a state of complete disorder, concurrent with a lower work-hardening rate. In fact,

Fig. 3

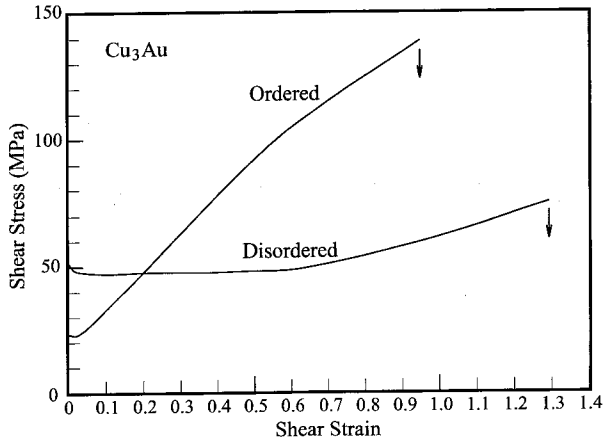

Shear stress–shear strain curves for Cu_3Au single crystals with a loading axis close to [321]. Fully ordered Cu_3Au exhibits a lower initial flow stress and strain hardens more rapidly than the same alloy in the macroscopically disordered state. Ordered Cu_3Au cooled $10°C\,day^{-1}$ from 400 to 280°C. Disordered Cu_3Au quenched from 450°C. (From Davis and Stoloff (1964).)

for $(Fe, Co)_3V$ ($L1_2$), Liu and Schulson (1984) suggested that the shearing kind of fracture at room temperature may be related to a loss in the degree of long-range order within the plastic zone around microcracks and to an attendant reduction in the work-hardening capacity, where the disordered $(Fe, Co)_3V$ work hardens at a rate of about one half of its hardening rate when fully ordered.

Fortunately, the essential material parameters are all known for Cu_3Au, in both the ordered and the disordered state. Thus in the current effort we concentrate on Cu_3Au to develop the essential arguments for the proposed analytical and finite-element models. Following this, similar arguments are advanced, by incorporating the relevant parameters for ordered Ni_3Al and other intermetallics, based on individual observations. For example, Ni_3Al exhibits a nearly linear work-hardening rate of 180 MPa (Aoki and Izumi 1978b) and exhibits uniform deformation (i.e. fine slip) for shear strain up to 0·6, suggesting complete order up to this level of shear strain. As the superpartial separations are shear strain dependent, they are embedded in finite-element procedures as strain against order, and consecutively work-hardening, parametric relations. The ensuing theoretical predictions are employed to predict intense localization effects in Ni_3Al single crystals. More specifically, experimental observations at the ångström length scale are used to explain macroscopic mechanical failures on a millimetre–centimetre length scale.

1.4. *Notation*

Standard tensor notation is used throughout. Bold symbols are used to denote vectors and higher-order tensors, the order of which will be clear in context. Inverses, transposes and transposed inverses are denoted with a superscript -1,T and $-$T respectively and superposed dots indicate differentiation with respect to time t. For example, if N_d is the number of spatial dimensions, then

$$\mathbf{c}\cdot\mathbf{d} = \sum_{i=1}^{N_d} c_i d_i \,, \quad \mathbf{cd} = \sum_{i=1}^{N_d}\sum_{j=1}^{N_d} c_i d_j \mathbf{b}_i\mathbf{b}_j \,, \quad \mathbf{B}\cdot\mathbf{c} = \sum_{i=1}^{N_d}\sum_{j=1}^{N_d} B_{ij} c_j \mathbf{b}_i$$

$$\mathbf{A}\cdot\mathbf{B} = \sum_{i=1}^{N_d}\sum_{j=1}^{N_d}\sum_{k=1}^{N_d} A_{ik}B_{kj}\mathbf{b}_i\mathbf{b}_j \,, \quad \mathbf{A} : \mathbf{B} = \sum_{i=1}^{N_d}\sum_{j=1}^{N_d} A_{ij}B_{ji} \,,$$

$$\mathbf{AB} = \sum_{i=1}^{N_d}\sum_{j=1}^{N_d}\sum_{k=1}^{N_d}\sum_{l=1}^{N_d} A_{ij}B_{kl}\mathbf{b}_i\mathbf{b}_j\mathbf{b}_k\mathbf{b}_l \,, \quad \mathbf{H} : \mathbf{A} = \sum_{i=1}^{N_d}\sum_{j=1}^{N_d}\sum_{k=1}^{N_d}\sum_{l=1}^{N_d} H_{ijkl}A_{lk}\mathbf{b}_i\mathbf{b}_j \,,$$

where the basis $\mathbf{b}_i$ is Cartesian and independent of time.

§ 2. Theoretical and numerical considerations

2.1. *Single crystal constitutive law*

The constitutive law can be written in a form similar to that developed by Hill and Rice (1972), Asaro and Rice (1977) and Asaro (1979), which is based on the early work of Taylor (1938). The constitutive framework has been applied and extended to study localized deformation modes in single crystals, e.g. Asaro and Rice (1977), Asaro (1979), Peirce, Asaro and Needleman (1982), Peirce *et al.* (1983), Qin and Bassani (1992a, b), and more recently Dao and Asaro (1993, 1996a, b).

Assume there are $\alpha = 1, 2 \ldots, N$ active slip systems. Slip system α is defined by orthogonal unit vectors $\mathbf{s}_\alpha, \mathbf{m}_\alpha$ and $\mathbf{z}_\alpha$, where $\mathbf{s}_\alpha$, is the current slip direction, $\mathbf{m}_\alpha$ is normal to the slip plane and $\mathbf{z}_\alpha$ is normal to both $\mathbf{s}_\alpha$ and $\mathbf{m}_\alpha$. The total deformation rate $\mathbf{D}$ and spin rate $\boldsymbol{\Omega}$ are given as

$$\mathbf{D} = \mathbf{D}^* + \sum_{\alpha=1}^{N} \mathbf{P}_\alpha \dot{\gamma}_\alpha, \quad \boldsymbol{\Omega} = \boldsymbol{\Omega}^* + \sum_{\alpha=1}^{N} \mathbf{W}_\alpha \dot{\gamma}_\alpha, \tag{1}$$

where $\mathbf{D}^*$ and $\boldsymbol{\Omega}^*$ are the elastic plus rigid-body rotation parts of $\mathbf{D}$ and $\boldsymbol{\Omega}$ respectively, and $\mathbf{P}_\alpha = (\mathbf{s}_\alpha \mathbf{m}_\alpha + \mathbf{m}_\alpha \mathbf{s}_\alpha)/2$ and $\mathbf{W}_\alpha = (\mathbf{s}_\alpha \mathbf{m}_\alpha - \mathbf{m}_\alpha \mathbf{s}_\alpha)/2$.

Following Dao and Asaro (1993), the general yield criterion is given as

$$\tau_\alpha + \boldsymbol{\eta}_\alpha : \boldsymbol{\sigma} = \mathbf{m}_\alpha \cdot \boldsymbol{\sigma} \cdot \mathbf{s}_\alpha + \boldsymbol{\eta}_\alpha : \boldsymbol{\sigma} = g_\alpha \tag{2}$$

where τ_α is the current value of the resolved shear stress, g_α is the current shear resistance, $\boldsymbol{\sigma}$ is the Cauchy stress and $\boldsymbol{\eta}_\alpha$ is the tensor of non-Schmid effects for slip system α which, when aligned with $\mathbf{s}_\alpha$, $\mathbf{m}_\alpha$ and $\mathbf{z}_\alpha$, takes the simple form

$$\boldsymbol{\eta} = \begin{bmatrix} \eta_{ss} & 0 & \eta_{sz} \\ 0 & \eta_{mm} & \eta_{mz} \\ \eta_{sz} & \eta_{mz} & \eta_{zz} \end{bmatrix}. \tag{3}$$

If the slip system α is to remain active, taking derivatives of both sides of eqn. (2) with respect to time t, we must have

$$\frac{\mathrm{d}(\mathbf{m}_\alpha \cdot \boldsymbol{\sigma} \cdot \mathbf{s}_\alpha + \boldsymbol{\eta}_\alpha : \boldsymbol{\sigma})}{\mathrm{d}t} = \sum_{\beta=1}^{N} h_{\alpha\beta} \dot{\gamma}_\beta, \tag{4}$$

where $h_{\alpha\beta}$ is a hardening matrix, the off-diagonal elements of which represent latent hardening. Asaro and Rice (1977) discussed various possibilities which differ in how lattice elasticity is accounted for, and almost the same results were obtained. For the present, we shall assume that $\mathbf{s}_\alpha$, $\mathbf{m}_\alpha$ and $\mathbf{z}_\alpha$ remain othorgonal unit vectors and simply rotate rigidly at the lattice spin rate $\boldsymbol{\Omega}^*$. Thus, in view of eqn. (3), after some rearrangements, we obtain

$$\frac{\mathrm{d}(\mathbf{m}_\alpha \cdot \boldsymbol{\sigma} \cdot \mathbf{s}_\alpha + \boldsymbol{\eta}_\alpha : \boldsymbol{\sigma})}{\mathrm{d}t} = \mathbf{Q}_\alpha : \overset{\nabla}{\boldsymbol{\sigma}}{}^*, \quad \mathbf{Q}_\alpha = \mathbf{P}_\alpha + \mathbf{T}^\alpha \cdot \boldsymbol{\eta} \cdot \mathbf{T}^{\alpha \mathrm{T}}, \tag{5}$$

where $\overset{\nabla}{\boldsymbol{\sigma}}{}^*$ is the Jaumann stress rate with respect to $\boldsymbol{\Omega}^*$, $\mathbf{T}^\alpha$ is the transformation tensor between laboratory axes $\mathbf{a}_i$ and the α slip system $\mathbf{s}_\alpha, \mathbf{m}_\alpha, \mathbf{z}_\alpha$, that is if $\mathbf{e}_1^\alpha = \mathbf{s}_\alpha, \mathbf{e}_2^\alpha = \mathbf{m}_\alpha, \mathbf{e}_3^\alpha = \mathbf{z}_\alpha$ then $T_{ij}^\alpha = \mathbf{a}_i \cdot \mathbf{e}_j^\alpha$.

Following the procedure used by Asaro (1979), we have the final constitutive equation

$$\overset{\nabla}{\boldsymbol{\sigma}} + \boldsymbol{\sigma} \mathrm{Tr}(\mathbf{D}) = \mathbf{L} : \mathbf{D} - \sum_{\alpha=1}^{N} \sum_{\beta=1}^{N} (\mathbf{L} : \hat{\mathbf{P}}_\alpha) N_{\alpha\beta}^{-1} (\mathbf{Q}_\beta : \mathbf{L} : \mathbf{D}), \tag{6a}$$

with

$$N_{\alpha\beta} = h_{\alpha\beta} + \mathbf{Q}_\alpha : \mathbf{L} : \mathbf{P}_\beta \text{ and } \hat{\mathbf{P}}_\alpha = \mathbf{P}_\alpha + \mathbf{L}^{-1} : (\mathbf{W}_\alpha \cdot \boldsymbol{\sigma} - \boldsymbol{\sigma} \cdot \mathbf{W}_\alpha), \tag{6b}$$

where $\overset{\nabla}{\boldsymbol{\sigma}}$ is the Jaumann stress rate with respect to $\boldsymbol{\Omega}$ and $\mathbf{L}$ is the elastic moduli.

A rate-dependent version of the single-crystal constitutive law can be obtained by using a rate-dependent flow rule, namely

$$\dot{\gamma}_\alpha = \dot{a}\,\mathrm{sgn}\,(\tau_\alpha)\left(\left|\frac{\tau_\alpha + \eta_\alpha : \tau}{g_\alpha}\right|\right)^{1/m}, \quad \dot{g}_\alpha = \sum_{\beta=1}^{N} h_{\alpha\beta}\dot{\gamma}_\beta, \tag{7}$$

where g_α is the current hardness of slip system α, m is the material rate sensitivity exponent (taken to be nearly rate independent as $m = 200$ in this study), and $\dot{a}$ is the reference shear rate (taken to be $0{\cdot}001\ s^{-1}$ in this study). Detailed development of the rate-dependent constitutive theory can be found in the paper by Dao and Asaro (1993) and is omitted here. The rate-dependent version of the constitutive law has been implemented by the explicit rate tangent method (Peirce *et al.* 1983) to solve full boundary value problems using the finite-element method.

2.2. *Critical conditions of localized deformation*

For materials described by idealized rate-independent constitutive laws, Hill (1962) has given a general theory of bifurcation of a homogeneous elastic–plastic flow field into bands of localized deformation. For this to occur there is first the kinematical restriction that for localization in a thin planar band with unit normal **n** (fig. 4) the velocity gradient field $\partial\mathbf{v}/\partial\mathbf{x}$ inside the band can differ from the velocity gradient field $\partial\mathbf{v}^0/\partial\mathbf{x}$ outside as

$$\frac{\partial\mathbf{v}}{\partial\mathbf{x}} - \frac{\partial\mathbf{v}^0}{\partial\mathbf{x}} = \mathbf{gn}. \tag{8}$$

In addition, there is the continuing equilibrium requirement that

$$\mathbf{n}\cdot\dot{\boldsymbol{\sigma}} = \mathbf{n}\cdot\dot{\boldsymbol{\sigma}}^0 = \mathbf{0} \tag{9}$$

at incipient localization where $\dot{\boldsymbol{\sigma}}$ is the stress rate inside the band and $\dot{\boldsymbol{\sigma}}^0$ that outside.

The constitutive law (6) together with the conditions for localization (8) and (9) can be solved to obtain critical conditions for the onset of localization. For single crystals undergoing single slip, Asaro and Rice (1977) gave the critical condition of shear bands that are nearly parallel to the slip plane:

Fig. 4

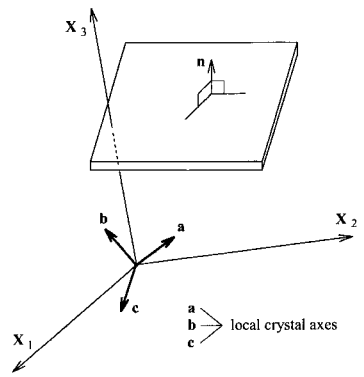

Cartesian coordinates and reference crystal axes **a**, **b** and **c**, where the right-hand triad **a**, **b** and **c** are some specific crystallographic directions of the single crystal. The surface of localization is shown with unit normal **n**.

$$h_{\mathrm{cr}} = \frac{1}{4}(\boldsymbol{\eta} : \mathcal{M}\cdot\mathbf{s})\cdot(\mathbf{s}\cdot\mathcal{M}\cdot\mathbf{s})^{-1}\cdot(\mathbf{s}\cdot\mathcal{M} : \boldsymbol{\eta}); \tag{10a}$$

these bands have the normal

$$\mathbf{n} \approx \mathbf{m} + \frac{1}{2}(\mathbf{s}\cdot\mathcal{M}\cdot\mathbf{s})^{-1}\cdot(\mathbf{s}\cdot\mathcal{M} : \boldsymbol{\eta}), \tag{10b}$$

where

$$\mathcal{M} = \mathbf{L} - (\mathbf{L}\cdot\mathbf{m})\cdot(\mathbf{m}\cdot\mathbf{L}\cdot\mathbf{m})^{-1}\cdot(\mathbf{m}\cdot\mathbf{L}). \tag{10c}$$

For single crystals undergoing multiple slip, Dao and Asaro (1996a) applied a general method for various three-dimensional slip geometries, where the critical conditions can be obtained by numerically solving the equation

$$\det(\mathbf{M}) = 0, \tag{11a}$$

with

$$\mathbf{M} = \mathbf{n}\cdot\mathbf{L}\cdot\mathbf{n} - \sum_{\alpha=1}^{N}\sum_{\beta=1}^{N}(\mathbf{n}\cdot\mathbf{L} : \hat{\mathbf{P}}_\alpha)N^{-1}_{\alpha\beta}(\mathbf{Q}_\beta : \mathbf{L}\cdot\mathbf{n}) + \mathbf{A}, \tag{11b}$$

where $\mathbf{A} = \{(\mathbf{n}\cdot\boldsymbol{\sigma}\cdot\mathbf{n})\mathbf{I} - \boldsymbol{\sigma} - (\mathbf{n}\cdot\boldsymbol{\sigma})\mathbf{n} - \mathbf{n}(\boldsymbol{\sigma}\cdot\mathbf{n})\}/2$ and $\mathbf{I}$ is the second-order identity tensor.

§ 3. A MODEL FOR INTENSE SHEAR FAILURE

3.1. *A general discussion on localized deformation in Ni_3Al*

We begin by illustrating two points: firstly the inability of non-Schmid arguments to explain the room-temperature localization effects, and consequently secondly the necessity to invoke a separate mechanism that may cause $h \to 0$.

The geometry of a single crystal undergoing single slip is shown in fig. 5(*a*), where the angle between the slip plane normal **m** and the normal **n** of the localiza-

Fig. 5

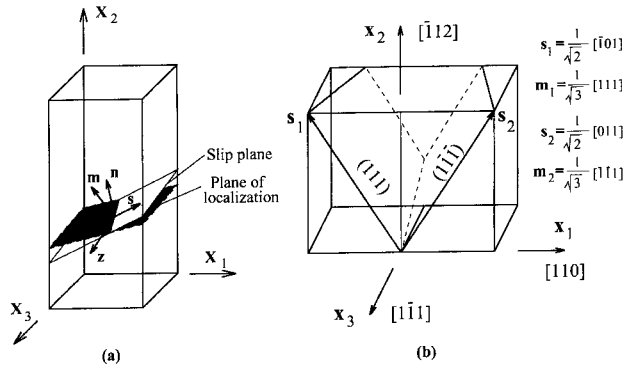

(*a*) Geometry of a single crystal undergoing single slip, where the angle between the slip plane normal **m** and the normal **n** of the localization is defined as the shear band misorientation angle. (*b*) Geometry of a Ll_2 (or fcc) single crystal undergoing double symmetric slip, with $[\bar{1}01](111)$ and $[011](\bar{1}\bar{1}1)$ as the primary and conjugate slip systems respectively, and with $[\bar{1}12]$ as the tensile axis.

tion plane is defined as the shear band misorientation angle. Figure 5(*b*) shows the geometry of a $L1_2$ (or fcc) single crystal undergoing double symmetric slip, with $[\bar{1}01](111)$ and $[011](\bar{1}\bar{1}1)$ as the primary and conjugate slip system respectively, and with $[\bar{1}12]$ as the tensile axis.

For Ni_3Al, let $\mathbf{s} = (1/2^{1/2})[\bar{1}01], \mathbf{m} = (1/3^{1/2})[111]$ and $\mathbf{z} = (1/6^{1/2})[\bar{1}2\bar{1}]$, and the Burgers vector $\mathbf{b} = (a/2)[\bar{1}01]$; thus τ_{sm} is the resolved shear stress on the primary (111) slip plane in the direction of the $(a/2)[\bar{1}01]$ Burgers vector **b**, and τ_{cb} is the resolved shear stress on the (010) cross-slip plane in the direction of the $(a/2)[\bar{1}01]$ Burgers vector. The estimated non-Schmid factors for Ni_3Al at several different temperatures are listed in the table 1 (Dao and Asaro 1993), and the critical condition of localization h_{cr}, under uniaxial tension, are listed in table 2. Room-temperature elasticity constants, that is $C_{11} = 223\,\text{GP}a$, $C_{12} = 148\,\text{GP}a$ and $C_{44} = 125\,\text{GP}a$ are used (Yoo 1987). The single-slip results are obtained from eqn. (10*a*), and the non-Schmid factors are those with $\tau_{sm} > 0$ and $\tau_{cb} > 0$ for simple tension. The double-slip results are obtained from solving eqn. (11*a*) for the geometry shown in fig.

Table 1. Non-Schmid factors for Ni_3Al at several temperatures.

Temperature (K)	Stress State	η_{ss}	η_{mm}	η_{zz}	η_{mz}	η_{sz}
293	$\tau_{sm} > 0, \tau_{cb} > 0$	0	0·008	−0·008	0·008	−0·015
	$\tau_{sm} < 0, \tau_{cb} < 0$	0	−0·008	0·008	−0·008	−0·015
	$\tau_{sm} > 0, \tau_{cb} < 0$	0	0·008	−0·008	0·008	0·014
	$\tau_{sm} < 0, \tau_{cb} > 0$	0	−0·008	0·008	−0·008	0·014
600	$\tau_{sm} > 0, \tau_{cb} > 0$	0	0·036	−0·036	0·037	−0·065
	$\tau_{sm} < 0, \tau_{cb} < 0$	0	−0·036	0·036	−0·037	−0·065
	$\tau_{sm} > 0, \tau_{cb} < 0$	0	0·030	−0·030	0·031	0·054
	$\tau_{sm} < 0, \tau_{cb} > 0$	0	−0·030	0·030	−0·031	0·054
800	$\tau_{sm} > 0, \tau_{cb} > 0$	0	0·046	−0·046	0·048	−0·083
	$\tau_{sm} < 0, \tau_{cb} < 0$	0	−0·046	0·046	−0·048	−0·083
	$\tau_{sm} > 0, \tau_{cb} < 0$	0	0·037	−0·037	0·038	0·067
	$\tau_{sm} < 0, \tau_{cb} > 0$	0	−0·037	0·037	−0·038	0·067

Table 2. Critical conditions of localization for Ni_3Al.

	Deformation mode	h_{cr} (MPa)	Misorientation (degrees)
Schmid's rule	Single slip	0	0
Schmid's rule	Double slip	35·6	0·3
Non-Schmid effects $T = 273\,\text{K}$	Single slip	28·4	0·9
Non-Schmid effects $T = 273\,\text{K}$	Double slip	52·8	1·0
Non-Schmid effects $T = 600\,\text{K}$	Single slip	520	3·7
Non-Schmid effects $T = 600\,\text{K}$	Double slip	430	4·1
Non-Schmid effects $T = 800\,\text{K}$	Single slip	840	4·7
Non-Schmid effects $T = 800\,\text{K}$	Double slip	700	5·1

5(*b*), where the tensile stress at the localization (right before failure) is taken as $\sigma_{22} = 600\,\text{MP}a$ (Aoki and Izumi 1978a).

From table 2, we note that firstly non-Schmid effects have important influences on the critical localization conditions, especially the critical hardening rate h_{cr}, and secondly the misorientation angles are very small for all cases (no more than 5·1°). It is clear that localized deformation is possible under positive material hardening (sometimes can be as high as 700–800 MP*a*), consistent with earlier findings (Asaro and Rice 1977, Dao and Asaro 1993). However, from table 1, we note that non-Schmid factors are quite small at room temperature. Thus, while the predicted misorientation angles (no more than 1°), coincide with the observed intensive shearing along the slip plane (see fig. 1), the predicted h_{cr} is of the order of 30–50 MPa, much smaller than the commonly observed hardening rate (200–700 MP*a* (Aoki and Izumi 1978a)) for Ni_3Al single crystals tested at room temperature. Thus, non-Schmid effects *alone* cannot explain the intense slip plane shear failure at room temperature.

The nature of localization can vary quite significantly with hardening rates. Figures 6(*a*), (*b*) and (*c*) shows finite-element calculations of typical localization modes at three hardening rates, $h = 0$, $0 < h = 0{\cdot}28h_{cr} < h_{cr}$ and $h = 1{\cdot}6h_{cr} > h_{cr}$ respectively, all at 1% strain. Note that we assume a uniform deformation mode at the beginning of the three 'computational experiments' shown in fig. 6, where the 1% strain represents the additional strain after some previous uniform deformation. In our two-dimensional finite-element calculations, the only non-zero non-Schmid factor is given as $\eta_{ss} = 0{\cdot}05$, and the elasticity is taken as isotropic with shear modulus $G = 100\,\text{GP}a$ and Poisson's ratio $\nu = \frac{1}{3}$. Single-slip deformation mode is assumed with the hardening rate h kept constant during the tensile loading. The critical hardening rate is calculated from eqn. (10*a*) as $h_{cr} = 187{\cdot}5\,\text{MPa}$. Finite-ele-

Fig. 6

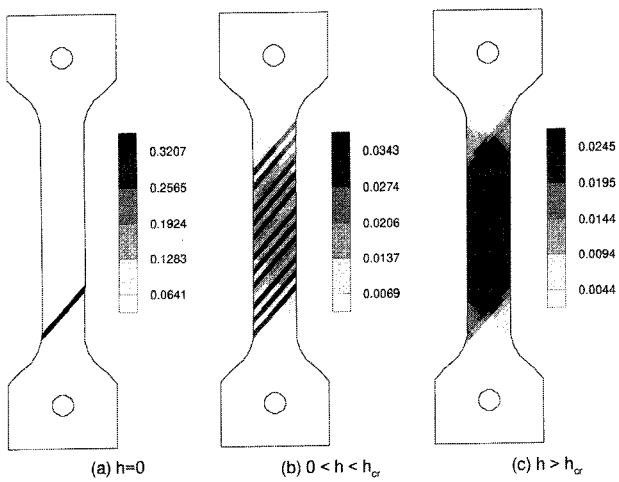

Finite-element calculations of typical localization modes at three hardening rates (*a*) $h = 0$, (*b*) $0 < h = 0{\cdot}28h_{cr} < h_{cr}$ and (*c*) $h = 1{\cdot}6h_{cr} > h_{cr}$, all at 1% additional strain assuming a uniform deformation mode at the beginning of the calculations.

ment computations show the following: for $h > h_{cr}$, there is no localization; for $0 < h < h_{cr}$ *course slip bands* (CSBs) form; for $h \to 0$, the localization tends to *persist* at the same location.

Thus a persistent intense shear band is possible *only* when the hardening rate approaches zero (or negative values). In the next section, we invoke the observation of Horton, Baker and Yoo (1991) of deformation-induced slip plane disordering that may reduce the strain hardening significantly and eventually result in intense shear banding.

3.2. *Effects of disordering on the mechanical behaviour*

The effects of disordering on the mechanical behaviour have been most adquately reported for Cu_3Au, which is isostructural with Ni_3Al. Thus mechanical response for a range of order conditions have been evaluated. Table 3 lists the matrix of mechanical responses and failure strains extracted from the literature, suggesting that disorder is essentially concomitant with a lower work hardening rate. Perhaps the best example of shear-strain-induced disorder is provided by Audero, Victoria and Vidoz (1969) for partially ordered Cu_3Au, where the initial high hardening rate (close to that of a fully ordered alloy) is gradually lowered following plastic deformation. These workers had surmised that plastic deformation destroys this low order condition, such that superdislocations present initially are replaced by unit dislocations, thereby resulting in a lower work-hardening rate.

Horton, Baker and Yoo (1991) provide the essential microscopy evidence, for 'localized' slip plane disordering in stoichiometric Ni_3Al, for the model described herein. In their work, experimental observations were made of the spacing of superpartial dislocations generated during *in-situ* deformation experiments, and recorded under stress. In the extensively deformed slip bands, the separations between superpartials get progressively larger until uncoupling occurs (fig. 7). The significantly larger separations (up to 15 nm, and uncoupled) measured in the slip bands imply a lower antiphase-boundary (APB) energy and consequently a lower degree of order in the deformed slip band. Analogous to the case of Cu_3Au, we assume that, as the

Table 3. Room-temperature mechanical properties of Cu_3Au and Ni_3Al: CRSS, critical resolved shear stress.

		Ordered		Disordered		
Material	Loading axis	CRSS (MPa)	h (MPa)	CRSS (MPa)	h (MPa)	Reference
Cu_3Au	Near [321]	22	175	48	$h_I \approx 0; h_{II} \approx 35$	Davis and Stoloff (1963, 1964)
Cu_3Au	[011]	28	150	50	$h_I \approx 0; h_{II} \approx 120$	Audero *et al.* (1969)
Cu_3Au	[321]	20	160	40	$h_I \approx 0; h_{II} \approx 60;$ $h_{III} \approx 20$	Chien and Starke (1975)
Ni_3Al	[321]	60	180	—	—	Aoki and Izumi (1978b)
Ni_3Al (1 at.%Ta)	[321]	45	300	—	—	Baluc (1990)

Fig. 7

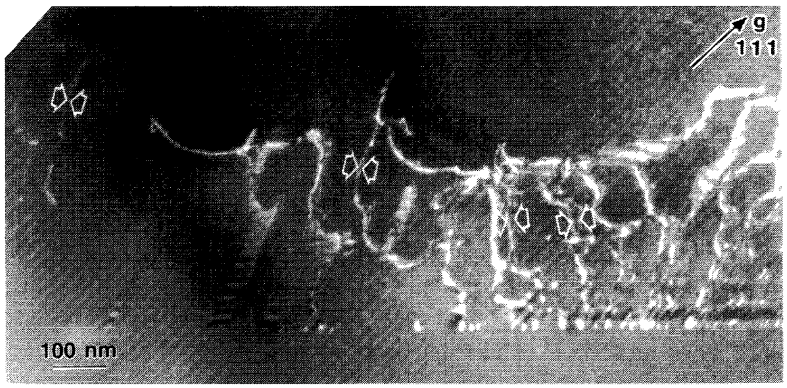

Micrograph of APB-coupled disloctions show a separation that depends on their position in a slip band (dark-field image of the lead dislocations). The separations of the arrowed dislocations from left to right are 4, 5, 10 and 15 nm respectively. (Photograph taken from Horton *et al.* (1991).)

APB energy term approaches zero (i.e. uncoupling of super-partials), it is a state of complete disorder, concurrent with a lower work-hardening rate.

Within the framework of the experimental evidence of Horton *et al.* (1991), we begin with the assumption that this localized order–disorder stress strain behaviour in Ni_3Al has similar features as macroscopically ordered and disordered Cu_3Au (see fig. 3). This underlying assumption is supported by the numerous and striking similarities in the deformation behaviours of Cu_3Au, Ni_3Fe (with low APB energy) and Ni_3Al (high APB energy) ordered $L1_2$ alloys. For example, each alloy in the ordered state exhibits a linear work-hardening rate, and a strong latent hardening effect for the secondary (conjugate) slip systems. The stress–strain behaviour lacks the stage I hardening, typical of disordered fcc single crystals. Instead, a strong linear hardening is observed initially, and slip occurs almost exclusively on the primary slip system. This primary slip system continues to operate, nearly up to fracture, even after the tensile axis overshoots beyond the [001]–[111] symmetry line in these alloys (Davies and Stoloff 1963, Victoria and Vidoz 1968, Chien and Starke 1975, Aoki and Izumi 1978b). Samples with near [321] tensile axis, oriented for single slip, exhibit similar shear strains at fracture. For example, a near [321] tensile axis in Cu_3Au gives a shear strain of about 1·2 (Chien and Starke 1975), and shear strains of about 1·5 were observed for Ni_3Fe (Victoria and Vidoz 1968) and Ni_3Al (Aoki and Izumi 1978b). A survey of room-temperature mechanical properties of Cu_3Au and Ni_3Al can be found in table 3, where h_I, h_{II} and h_{III} represent stage I, II and III shear strain hardening values respectively.

Accordingly, the model behaviour of Ni_3Al single crystals is shown in fig. 8, where the critical resolved shear stresses for ordered and disordered crystals are given as $\tau_o = 60$ MPa and $\tau_d = 120$ MPa respectively, and the hardening rates for ordered and disordered crystals are given as $h_o = 200$ MPa and $h_d = 40$ MPa respectively. We take the simplest case where disordering initiates at shear strain γ_e and becomes fully disordered at shear strain γ_e, with the long-range order X_{LRO} varying linearly from 1·0 at γ_0 to 0 at γ_c, that is

Fig. 8

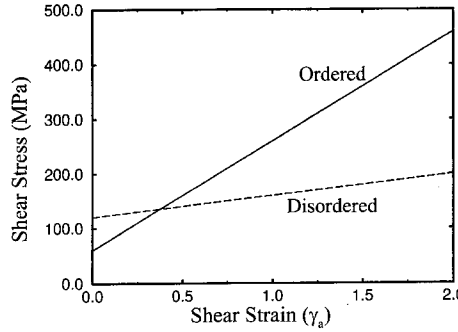

Simple linear hardening used in modelling ordered and disordered Ni_3Al single-crystal behaviour. Analogous to the case of Cu_3Au, the essential feature is that fully ordered Ni_3Al exhibits a lower initial flow stress and strain hardens more rapidly than the same alloy in the macroscopically disordered state.

$$X_{\mathrm{LRO}} = \frac{\gamma_e - \gamma_a}{\gamma_e - \gamma_0} \quad (\gamma_0 \leqslant \gamma_a \leqslant \gamma_e). \tag{12}$$

Furthermore, employing a simple rule of mixture, the single-crystal shear stress–shear strain behaviour can be expressed as

$$\tau = \begin{cases} \tau_o + h_o\gamma_a, \\ X_{\mathrm{LRO}}(\tau_o + h_o\gamma_a) + (1 - X_{\mathrm{LRO}})(\tau_d + h_d\gamma_a), \end{cases} \quad \text{if} \begin{cases} \gamma_a < \gamma_0, \\ \gamma_0 \leqslant \gamma_a \leqslant \gamma_e, \end{cases} \tag{13}$$

where the material is assumed to fail before γ_e. Figure 9 shows the shear stress–shear strain curves computed using eqns. (12) and (13) with different combinations of γ_0 and γ_e, where all curves demonstrate a decreasing hardening rate. Thus, irrespective

Fig. 9

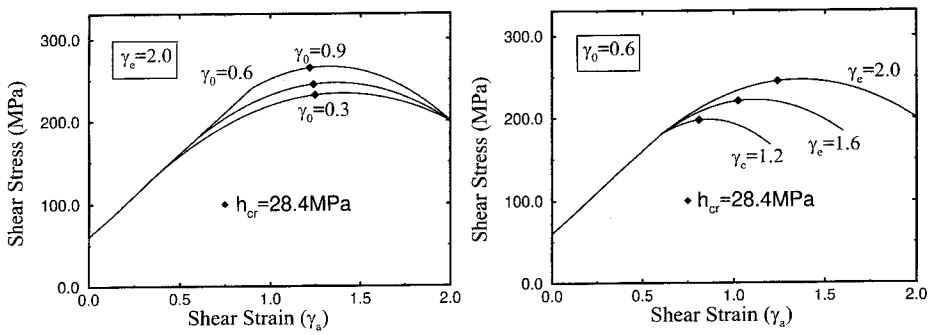

Shear stress–shear strain curves computed using eqns. (12) and (13) with different combinations of γ_0 and γ_e. Irrespective of the specificity of the disordering function $X_{\mathrm{LRO}}(\gamma_a)$, including the initiation and ending shear strains γ_0 and γ_e, and/or the mixture rules employed, we approach a saturation (and even negative) work-hardening behaviour essential for localization. The full diamonds show the starting points where $h \leqslant h_{cr}$.

of the specificity of the disordering function $X_{LRO}(\gamma_a)$, including the initiation and ending shear strains γ_0 and γ_e, and/or the mixture rules employed, we approach a saturation (and even negative) work-hardening behaviour essential for localization.

3.3. *Specific modelling for Ni_3Al shear failure: local disordering*

Sections 3.1. and 3.2. provide the essential backdrop for embedding the relevant experimental parameters available for Ni_3Al. A reasonable measure of prior strain for the onset of local disorder is required. Unfortunately, Horton *et al.* (1991) do not provide a measure of *in-situ* strain for their microscopy evidence. However, optical microscopy evidence of surface slip features (Aoki and Izumi 1978b) indicates fine and homogeneous slip for shear strains up to 0·6 (just prior to the [001]–[111] symmetry line) in Ni_3Al single crystals, with conjugate slip being activated at about 1·2 shear strain. Supplemental evidence for Cu_3Au ordered single crystals also indicate homogeneous slip for shear strains up to 0·6 (Davies and Stoloff 1963). Thus disordering is estimated to initiate at 0·6, and complete disordering occurs linearly over an additional shear strain of 1. This large magnitude of localized strain may be realized well before the macroscopic failure strain of 1·2.

A two-dimensional model crystal is used in the finite-element calculation run with $h_{cr} = 28{\cdot}4\,\text{MPa}$ ($\eta_{ss} = 0{\cdot}0194$; $G = 100\,\text{GPa}$; $\nu = \frac{1}{3}$). Since the deformation is essentially uniform before the $h = h_{cr}$ point in fig. 10, the finite-element calculation is initiated at this critical point assuming uniform material properties in the crystal. The deformation mode is set to be single slip with a 40° angle between the tensile axis and the slip plane, in close correlation with the actual testing configuration of Aoki and Izumi (1978b).

§ 4. Results and discussion

Figure 10 shows the shear stress–shear strain behaviour of a model Ni_3Al single crystal, where $\gamma_0 = 0{\cdot}6$ and $\gamma_e = 1{\cdot}6$. The open triangle indicates the point where the hardening rate drops to $h = h_{cr} = 28{\cdot}4\,\text{MPa}$ (room-temperature single-slip case in table 2). Figures 11 (*a*), (*b*) and (*c*) shows the deformed mesh, the accumulated shear strain (additional beyond $h = h_{cr}$) and lattice rotation (in degrees, positive values show counter-clockwise rotation), after an additional 3·9% tensile strain beyond the

Fig. 10

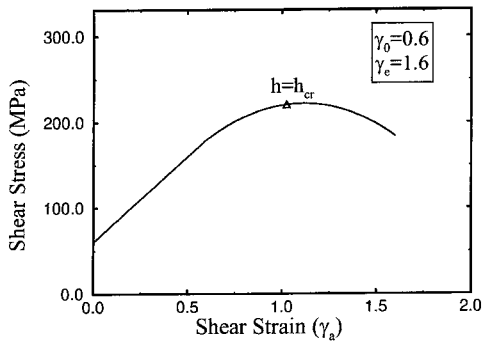

Shear stress–shear strain behaviour of the model Ni_3Al single crystal used in the finite-element calculation. The open triangle labelled $h = h_{cr}$ is the shear band initiation point.

Fig. 11

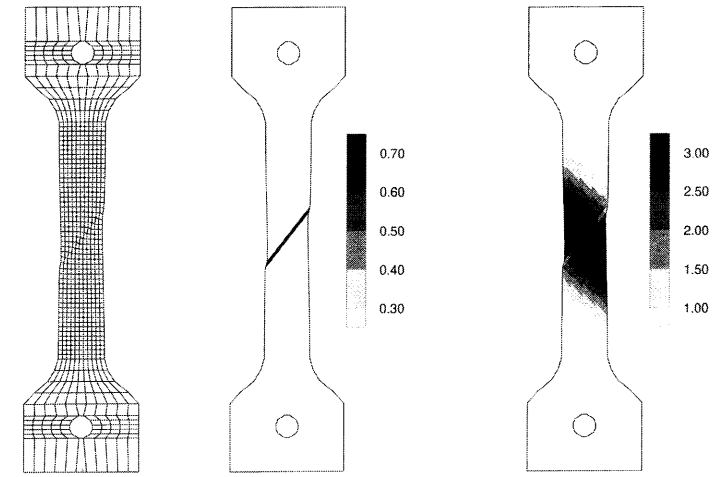

Finite-element calculation results: (*a*) deformed mesh; (*b*) accumulated shear strain (additional beyond $h = h_{cr}$); (*c*) lattice rotation (in degrees; positive values show counter-clockwise rotation), after an additional 3·9% tensile strain beyond the $h = h_{cr}$ point. The intense shearing can be seen clearly in (*a*) and (*b*). The lattice rotation across the shear band is very small (less than 1·5°) in (*c*).

$h = h_{cr}$ point, respectively. The intense shearing can be seen clearly in figs. 11 (*a*) and (*b*). The lattice rotation across the shear band is very small (less than 1·5°) in fig. 11 (*c*). Figure 12 shows the slip trace vectors of each element, showing that the shear band is nearly parallel to the slip plane. A similar scenario is expected under double- or multiple-slip modes because, once the localization initiates at a plane nearly

Fig. 12

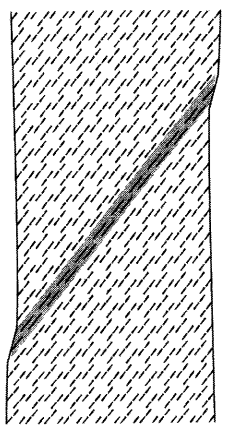

Slip trace vectors of each finite element, showing that the shear band is nearly parallel to the slip plane.

parallel to the slip plane (cf. table 2) under a double-slip or multiple-slip mode, the shear strain inside the band builds up very quickly which again leads to the very intense shearing before failure, as long as there is disordering driven by straining.

In most intermetallic compounds, including Ni_3Al, the material hardening is fairly high and stable during the deformation at room temperature. Looking back to § 3.1, we reiterate that such a high hardening certainly cannot result in any persistent shear bands, even with large non-Schmid effects, and a separate mechanism, that decreases the hardening rate to near zero or even negative values, is required. Strain-induced local disordering is a viable mechanism, consistent with experimental observations. Table 2 shows that relatively small non-Schmid factors ($\mathcal{O}(0{\cdot}01)$) can raise the critical hardening rate significantly to a value above zero (30–50 MPa). However, in the context of the current model, it appears that non-Schmid effects are not a necessary prerequisite for intense slip plane shear failures observed at ambient temperatures. Intense slip plane shear failures are still possible under the multiple-slip deformation mode, although non-Schmid effects may initiate the catastrophic shearing much earlier. Therefore, our model concept is quite general and should be applicable to other intermetallics as well.

§ 5. Summary

A model for intense slip plane shear failure is proposed for Ni_3Al and shown to be consistent with experimental evidences. The geometry of localized shear bands in single crystals (i.e. small misorientation angle between the slip plane and the plane of localization) is found to be responsible for the sharp and intense failure surfaces that are nearly parallel to the slip planes. The order–disorder transition driven by large shear strain provides the requisite mechanism to drive the hardening rate to nearly zero and/or negative values essential for the persistent localizations observed in Ni_3Al single crystals.

Acknowledgements

Selected computations were performed at the San Diego Supercomputer Center. B.K.K. thanks Dr C. T. Liu for bringing the problem to his attention during a conversation at the Third International Conference on High Temperature Intermetallics, held at San Diego in May 1994. The authors gratefully acknowledge helpful discussions with Dr J. H. Horton and Dr Patrick Veyssière during the course of this study.

References

Aoki, K., and Izumi, O., 1978a, *Acta Metall.*, **26**, 1257; 1978b, *Trans. Japan Inst. Metals*, **19**, 145.

Asaro, R. J., 1979, *Acta metall.*, **27**, 445.

Asaro, R. J., and Rice, J. R., 1977, *J. Mech. Phys. Solids*, **25**, 309.

Audero, M. A., Victoria, M. P., and Vidoz, A. E., 1969, *Phys. Stat. sol*, **31**, 697.

Baker, I., Horton, J. A., and Schulson, E. M., 1987, *Phil. Mag. Lett.*, **55**, 3.

Baluc, N., 1990, PhD Thesis, Ecole Polytechnique Fédérale Lausanne.

Beevers, C. J., and Honeycombe, R. W., 1962, *Acta metall.*, **10**, 17.

Chang, Y. W., and Asaro, R. J., 1981, *Acta metall.*, **29**, 241.

Chien, K. H., and Starke, E.A. Jr., 1975, *Acta metall.*, **23**, 1173.

Dao, M., and Asaro, R. J., 1993, *Mater. Sci. Engng.* A, **170**, 143; 1996a, *Mech. Mater.* (to be published); 1996b *Ibid.* (to be published).

Davis, R. G., and Stoloff, N. S., 1963, *Acta metall.*, **11**, 1187; 1964, *Phil. Mag.* A, **29**, 349.

Duffy, J., 1991, *J. Phys., Paris, IV*, **I**, 645.

ELAM, C. F., 1925, *Proc. R. Soc.* A, **109**, 143.
GILMAN, J. J., 1994, *Mech. Mater.*, **17**, 83.
HARREN, S. V., DÈVE, H. E., and ASARO, R. J., 1988, *Acta metall.*, **36**, 2435.
HILL, R., 1962, *J. Mech. Phys. Solids*, **10**, 1.
HILL, R., and RICE, J. R., 1972, *J. Mech. Phys. Solids*, **20**, 401.
HORTON, J. A., BAKER, I., and YOO, M. H., 1991, *Phil. Mag.* A, **63**, 319.
LIU, C. T., and SCHULSON, E. M., 1984, *Metall. Trans.* A, **15**, 701.
PAIDAR, V., POPE, D. P., and VITEK, V., 1984, *Acta metall.*, **32**, 435.
PEIRCE, D., ASARO, R. J., and NEEDLEMAN, A., 1982, *Acta metall.*, **30**, 1087; 1983, *Ibid.*, **31**, 1951.
PRICE, R. J., and KELLY, A., 1964, *Acta metall.*, **12**, 974.
QIN, Q., and BASSANI, J. L., 1992a, *J. Mech. Phys. Solids*, **40**, 813; 1992b, *Ibid.*, **40**, 835.
SACHS, G., and WEERTS, H., 1931, *Z. Phys.*, **67**, 507.
TAKEUCHI, S., and KURAMOTO, E., 1973, *Acta metall.*, **21**, 415.
TAYLOR, G. I., 1938, *Stephen Timoshenko 60th Anniversary Volume* edited by J. M.Lessels (London: Macmillan), p. 218.
VICTORIA, M., and VIDOZ, A. E., 1968, *Phys. Stat. sol.*, **28**, 131.
VIDOZ, A. E., LAZAREVIC, D., and CAHN, R. W., 1963, *Acta metall.*, **11**, 17.
WECHSLER, M. S., 1973, *The Inhomogeneity of Plastic Deformation* edited by R. E. Reed-Hill (Metals Park, Ohio: American Society of Metals), p.19.
YOO, M. H., 1987, *High-Temperature Ordered Intermetallic Alloys II*, edited by N. S. Stoloff, C. C. Koch, C. T. Liu and O. Izumi, Symposium Proceedings, Vol. 81, (Pittsburgh, Pennsylvania: Materials Research Society), p. 207.